

A balloon lens: Acoustic scattering from a penetrable sphere

Derek C. Thomas, Kent L. Gee, and R. Steven Turley

Citation: *American Journal of Physics* **77**, 197 (2009); doi: 10.1119/1.3041420

View online: <http://dx.doi.org/10.1119/1.3041420>

View Table of Contents: <http://scitation.aip.org/content/aapt/journal/ajp/77/3?ver=pdfcov>

Published by the [American Association of Physics Teachers](#)

WebAssign®

Free Physics Videos

Add these videos and many more resources — free with WebAssign.

bit.do/PhysicsResources



A balloon lens: Acoustic scattering from a penetrable sphere

Derek C. Thomas,^{a)} Kent L. Gee, and R. Steven Turley

Department of Physics and Astronomy, Brigham Young University, Provo, Utah 84602

(Received 6 February 2008; accepted 13 November 2008)

A balloon filled with a gas that has a different sound speed than that of air has been used as an acoustic lens. One purpose of the lens is to show refraction of sound waves in an analogy to geometric optics. We discuss the physics of the balloon lens demonstration. To determine the validity of a gas-filled balloon as a classroom demonstration of an acoustic lens and to understand the corresponding phenomena, its physics is considered analytically, numerically, and experimentally. Our results show that although a geometric analogy is a good first-order approximation, scattering theory is required to fully understand the observed phenomena. Thus this demonstration can be adapted to a wide range of students, from those learning the basic principles of refraction to advanced students studying scattering. © 2009 American Association of Physics Teachers. [DOI: 10.1119/1.3041420]

I. INTRODUCTION

The acoustic lens is suggested as a demonstration on many websites and is used in various science museums. The demonstration usually consists of a large balloon filled with a gas with a slower sound speed than air such as carbon dioxide.^{1,2} The balloon may be used in a whispering gallery type demonstration where a sound source on one side of the balloon is clearly heard by a listener at the focal point on the opposite side. Davy and Blackstock considered the effect of a gas-filled bubble on wave propagation.³ Their paper was primarily experimental in nature, their measurements were confined to the axis of the bubble, and they did not consider the possible classroom applications.

Many of the available explanations of the balloon lens (especially those available on the internet⁴) are either overly simplistic or misleading. This paper presents a more complete explanation of the physics of a balloon lens along with experimental, numerical, and analytical results.

II. THE BALLOON AS A LENS

Sound is the name given to small disturbances of the local pressure. In many cases these disturbances can be modeled by assuming that the total pressure P at any point is equal to the constant atmospheric pressure P_0 plus a small space and time dependent acoustic pressure fluctuation p such that $P = P_0 + p$. The acoustic pressure fluctuations or waves propagate at the speed of sound. In an ideal gas the speed of sound c is given by

$$c = \sqrt{\frac{\gamma P_0}{\rho_0}}, \quad (1)$$

where γ is the ratio of specific heats, P_0 is the equilibrium (atmospheric) pressure, and ρ_0 is the equilibrium density. As the density of the gas increases, the speed of sound decreases. Fermat's principle requires that a wave travel the shortest possible time-path. This requirement gives rise to Snell's law, which states that a ray parallel to the direction of energy propagation will bend at an interface between two media with different sound speeds:

$$\frac{1}{c_1} \sin \theta_1 = \frac{1}{c_2} \sin \theta_2, \quad (2)$$

where θ_1 is the angle from the surface normal of the incident wave and c_1 is the wave speed on the incident side of the interface; θ_2 is the angle from the surface normal of the transmitted wave and c_2 is the wave speed on the transmitted side.⁵ The standard method for using Eq. (2) to find the focal point of the lens is known as the paraxial approximation. This approximation assumes that the refracted rays deviate only slightly from the initial incident rays and replaces all trigonometric functions used to calculate the focal point with small angle approximations. Using this assumption, the standard lens equations may be derived. The focal length, q , of a spherical or ball lens, measured from the center of the lens, is found to be

$$q = \frac{na}{2(n-1)}, \quad (3)$$

where $n = c_1/c_2$ is the index of refraction and a is the radius of the lens. For example, the focal length of a carbon dioxide-filled balloon ($c_2 \approx 258$ m/s for carbon dioxide and $c_1 \approx 343$ m/s for air) with $a = 0.3$ m would be 0.61 m from the center of the balloon. This explanation of the balloon lens is the simplest and the one most suited in an introductory setting. However, it is limited, and for a spherical lens the focal point is much closer than is predicted by the paraxial approximation.

A better approximation can be found by using Eq. (2) to calculate the path of each ray. Inaccuracies are to be expected when using this ray tracing method for audible sound and a typically sized balloon because the method assumes that the wavelength is much smaller than the dimensions of the refracting object. This assumption is valid for an optical lens; a lens for light with a wavelength of 500 nm (green) would have a diameter of 1 cm. Achieving a similar ratio of lens dimension to wavelength for audible sound with a frequency equal to 1000 Hz (wavelength equal to 0.26 m) would require a lens 5 km in diameter. Although the ray tracing prediction is better if ultrasound is used, the demonstration is more impressive if the sound is in the audible range.

Although the analogy to an optical lens provides a first-order approximation, we will show that to predict the behav-

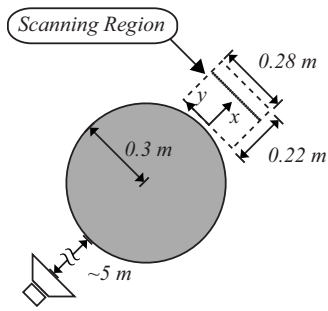


Fig. 1. Sketch of experimental setup used to measure the focusing effects of the balloon.

ior of an acoustic lens accurately requires more advanced methods. This paper is meant to fill a void for physics teachers and students by providing a more complete description of the physical principles and by suggesting how the balloon lens may be used as a demonstration in more advanced settings. We present experimental results that illustrate the characteristics of the sound field, numerical methods appropriate for a junior/senior level course in computational physics, and analytical results that employ methods typically introduced at the graduate level.

III. EXPERIMENTAL SETUP AND RESULTS

An experiment was performed to characterize the balloon's behavior and test the predictions of the equation for a ball lens. An approximately spherical balloon with a radius of 0.3 m was filled with carbon dioxide and placed in an anechoic chamber to minimize reflections of the acoustic waves. A Mackie HR824 studio monitor radiating white noise was placed 5 m away from the balloon. Placement of the balloon in the far field of the speaker resulted in nearly planar wavefronts incident on the balloon. An array of Larson Davis Type-1 0.5 in. microphones spaced at 12.7 cm intervals along the axis of the balloon was used to make preliminary measurements of the location of the focal point. Using this array, we determined that the focal region was approximately 0.10 m from the edge of the balloon. If the balloon is treated as a ball lens, the focal point would be located 0.32 m from the edge of the balloon. Ray tracing predicts that the focal region of the balloon lens should be approximately 0.20 m from the edge of the balloon. To resolve the details of the focal region of the balloon lens, a linear array of 23 GRAS Type-1 0.25 in. microphones spaced at 1.27 cm intervals was used to scan from approximately 5 to 27 cm from the balloon, for a total scanning area of $0.22 \text{ m} \times 0.28 \text{ m}$ (see Fig. 1).

Results of the microphone scans are presented as a function of the dimensionless parameter ka , where $k=2\pi/\lambda=2\pi f/c$ is the acoustic wavenumber in air, and a is the radius of the balloon. As can be seen in Fig. 2(a) for $ka=17.5$ ($f=3.18$ kHz) there is a peak in the sound pressure level at $x/\lambda \approx 0.75$, $y/\lambda \approx 0.3$ which seems to correspond to a focal point. However, according to the ball lens analogy, the focal point should be at $x/\lambda \approx 5.7$, and for the ray tracing method, the focal region should be at $x/\lambda \approx 2.4$. There also are two small lobes on the edges of the scanning region that are not predicted by treating the balloon as a simple acoustic

lens. The lobes are not symmetric within the measurement aperture because of the errors in balloon positioning. The lobes become more pronounced and more numerous as the frequency increases, as is apparent in Fig. 2(b), which is a plot of the same region for $ka=27.5$ ($f=5000$ Hz). The location of the focal region also changes between $ka=17.5$ and $ka=27.5$, which is not predicted by the lens equation or ray tracing. Because these results differ significantly from the predictions of the lens model, further investigation is required to see if the experiment is flawed or if a more accurate model is needed to describe the behavior of the balloon.

IV. NUMERICAL METHODS AND RESULTS

As a first step in validating the experimental results, the behavior of sound waves incident on a penetrable balloon was studied numerically. By penetrable, we mean that pressure waves may travel through the balloon, that is, the balloon is not rigid. The transmission loss as the wave travels through the balloon is neglected. A discussion of the vibration of spherical shells, which may serve as an appropriate model of vibrations on the balloon surface, is given in Ref. 5. To reduce the computational requirements the problem was reduced from three to two dimensions by treating the balloon as a circular region with the sound speed and density of carbon dioxide at the center of a two-dimensional grid that has the properties of air outside the circular region. This approach changes the problem from a penetrable sphere to an infinitely long, penetrable cylinder of the same radius and thus does not allow quantitative comparisons between the analytical, experimental, and numerical results. However, this simplification reduces the computation time substantially, which is very important if implemented in a class setting, simplifies coding, and still permits qualitative comparisons of features such as the number of lobes and the basic characteristics of the pressure field.

We begin with the classical wave equation for acoustic pressure in two-dimensional Cartesian coordinates,

$$\frac{1}{c^2} \frac{\partial^2 p}{\partial t^2} = \frac{\partial^2 p}{\partial x^2} + \frac{\partial^2 p}{\partial y^2}, \quad (4)$$

where c is the speed of sound and p is the pressure. Because the atmospheric pressure P_0 is assumed to be constant, it is only necessary to consider the acoustic pressure p instead of the total pressure P . Equation (4) is solved using a staggered leapfrog algorithm,⁶ which is accurate to second order in both space and time and is suitable for an undergraduate course in computational physics.

The solution of Eq. (4) produces a step-by-step picture of the time evolution of the pressure field (see Fig. 3). This feature can be highly educational, but it does not provide a ready comparison between the numerical and experimental results because the experiment is time averaged. To compare the numerical results to the experiment, the numerical grid was sampled at points corresponding to virtual microphones. These results were then time averaged to produce the plots in Figs. 2(c) and 2(d) for $ka=17.5$ and $ka=27.5$, respectively. A comparison of Figs. 2(c) and 2(d) with Figs. 2(a) and 2(b) shows that the results are very similar and that the numerical model predicts the occurrence of lobes as observed in the

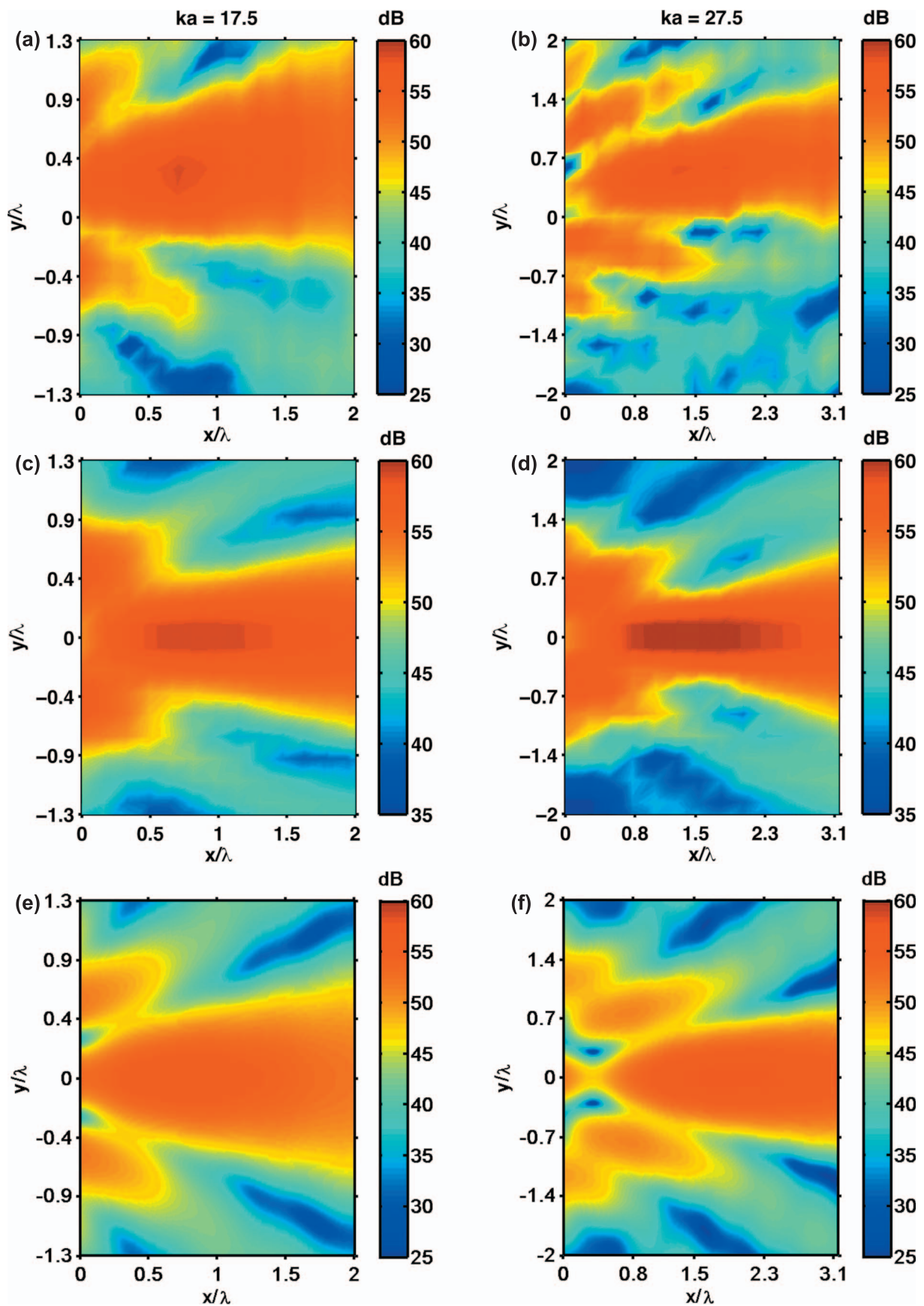


Fig. 2. The acoustic pressure field plotted over the region for $ka=17.5$ and $ka=27.5$: (a) and (b) are experimental measurements, (c) and (d) were obtained numerically, and (e) and (f) were produced using the analytical solution. The axes are normalized by the wavelength.

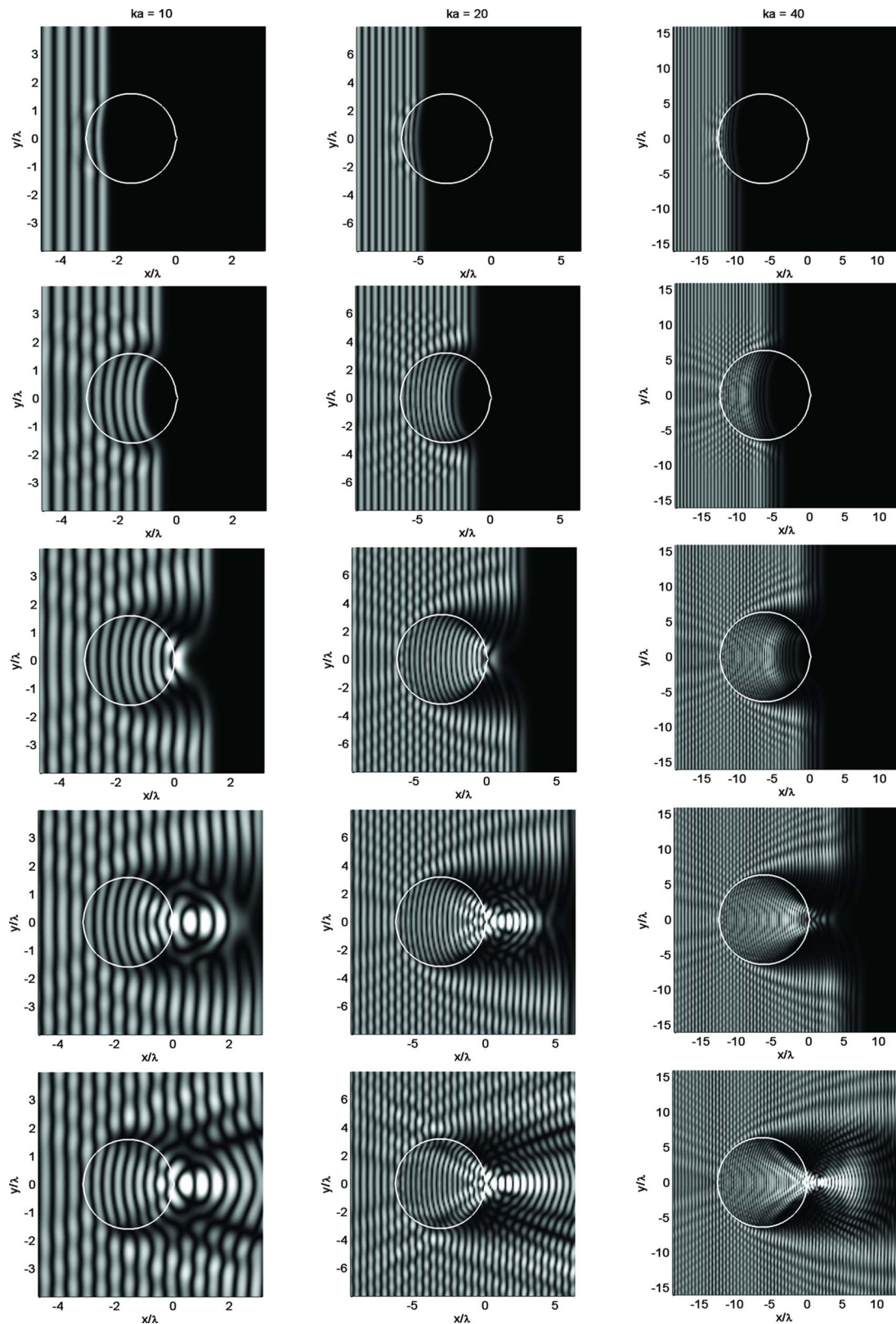


Fig. 3. Results of a numerical calculation of a plane wave incident on a circular penetrable scatterer for $ka=10$, $ka=20$, and $ka=40$.

experimental results. The numerical results indicate that the lobes and focal region are caused by the differing sound speeds of the two gases and not by other phenomena present in the experiment. However, the numerical experiment does not provide a deeper physical explanation of the phenomena.

V. ANALYTICAL METHODS AND RESULTS

Although the balloon lens has been used as a refraction demonstration primarily in introductory physics courses, more advanced mathematical methods are necessary to

describe the phenomenon analytically. The interaction between waves and objects with dimensions on the order of a wavelength is described by Mie scattering, which is discussed only in graduate level courses. For this problem a series solution to Mie scattering is adequate; for a more general approach using the Helmholtz integral see Ref. 7.

The case of a plane wave incident on a spherical balloon is considered. The exterior acoustic pressure p_e is given by the sum of the incident field p_i and the scattered field p_s . The interior quantities of the balloon are denoted by a subscript b and the radius of the balloon is a . Two conditions are used to relate the exterior and interior fields. The pressure field at the boundary is equal on both sides except for an arbitrary constant pressure difference Δp due to the pressurization of the gas inside the balloon:

$$[p_i + p_s]_{r=a} = p_b|_{r=a} + \Delta p. \quad (5)$$

The normal components of the velocity u of the interior and exterior fields are continuous at the boundary. To express this assumption in terms of the acoustic pressure, the linearized Euler's equation,⁸ $-\nabla p = \rho \partial u / \partial t$, a form of Newton's second law, is used. We use this relation to express the velocity boundary condition as

$$\left. \frac{1}{\rho} \frac{\partial p_e}{\partial \hat{n}} \right|_{r=a} = \left. \frac{1}{\rho_b} \frac{\partial p_b}{\partial \hat{n}} \right|_{r=a}, \quad (6)$$

where $p_e = p_i + p_s$ and $\partial / \partial \hat{n}$ represents the derivative with respect to the surface normal. As was the case for the numerical model, these assumptions neglect any shear waves in the balloon surface as well as any transmission loss through the balloon. These assumptions are justified by the agreement of the analytical and experimental results.

Our problem requires the solution of the classical wave equation for the acoustic pressure ($c^2 \nabla^2 p = \partial^2 p / \partial t^2$). It is useful to employ spherical coordinates instead of Cartesian coordinates. For the time harmonic excitation $\hat{p}(x, t) = p(x) e^{-i\omega t}$, the wave equation can be rewritten as the scalar Helmholtz equation,

$$(\nabla^2 + k^2)p = 0. \quad (7)$$

The scalar Helmholtz equation must be satisfied both inside and outside the balloon, with the constraint that the solutions be continuous and differentiable at the surface of the balloon.

An appropriate set of basis functions that satisfy the scalar Helmholtz equation in a spherical coordinate system includes the spherical Bessel functions (written in terms of the ordinary Bessel functions J and N)

$$j_m(x) = \sqrt{\frac{\pi}{2x}} J_{m+1/2}(x), \quad (8)$$

$$y_m(x) = \sqrt{\frac{\pi}{2x}} N_{m+1/2}(x), \quad (9)$$

and the normalized spherical harmonics,

$$Y_n^m(\phi, \theta) = \sqrt{\frac{2n+1}{4\pi} \frac{(n-m)!}{(n+m)!}} P_n^m(\cos \theta) e^{im\phi}, \quad (10)$$

where P_n^m represents the associated Legendre polynomials.⁹

A plane wave can be expressed in Cartesian coordinates as $p_i = p_0 e^{i\mathbf{k} \cdot \mathbf{r}}$, where \mathbf{k} is a vector of magnitude k oriented in the direction of propagation, \mathbf{r} is the position vector, and p_0 is the amplitude of the incident plane wave. In spherical coordinates the incident plane wave must be expanded as

$$p_i = p_0 e^{i\mathbf{k} \cdot \mathbf{r}} = 4\pi p_0 \sum_{n=0}^{\infty} \sum_{m=-n}^n i^n j_n(kr) Y_n^m(\phi, \theta) [Y_n^m(\phi_k, \theta_k)]^*, \quad (11)$$

where ϕ_k and θ_k indicate the direction of wave propagation, and the asterisk denotes the complex conjugate. With the balloon centered at the origin, the incident pressure evaluated at the surface of the balloon is

$$p_i|_{r=a} = 4\pi p_0 \sum_{n=0}^{\infty} \sum_{m=-n}^n i^n j_n(ka) Y_n^m(\phi, \theta) [Y_n^m(\phi_k, \theta_k)]^*. \quad (12)$$

The scattered and transmitted waves will have a similar form. Thus the scattered field at the boundary is

$$p_s|_{r=a} = \sum_{n=0}^{\infty} \sum_{m=-n}^n A_{mn} h_n^{(1)}(ka) Y_n^m(\phi, \theta), \quad (13)$$

where a is a constant and the spherical Hankel function of the first kind $h_n^{(1)} = j_n + iy_n$ is used to satisfy the Sommerfeld radiation condition,⁸ which requires that the scattered field approach zero at infinity. Similarly, the interior field at the boundary is

$$p_b|_{r=a} = \sum_{n=0}^{\infty} \sum_{m=-n}^n B_{mn} j_n(k_b a) Y_n^m(\phi, \theta), \quad (14)$$

where the spherical Bessel function of the first kind is used so that the field remains bounded at the origin.

Due to the orthogonality of the spherical harmonics, the coefficients A_{mn} and B_{mn} may be equated term by term to find that

$$A_{00} = \frac{2p_0 \sqrt{\pi} [k_b \rho j_0'(k_b a) j_0(ka) - k \rho_b j_0'(ka) j_0(k_b a)] - k_b \rho j_0'(k_b a) \Delta p}{k \rho_b h_0^{(1)'}(ka) j_0(k_b a) - k_b \rho h_0^{(1)}(ka) j_0'(k_b a)}, \quad (15)$$

$$A_{mn} = 4\pi p_0 i^n [Y_n^m(\phi_k, \theta_k)]^* \frac{k_b \rho j_n'(k_b a) j_n(ka) - k \rho_b j_n'(ka) j_n(k_b a)}{k \rho_b h_n^{(1)'}(ka) j_n(k_b a) - k_b \rho h_n^{(1)}(ka) j_n'(k_b a)} \quad (m, n \neq 0), \quad (16)$$

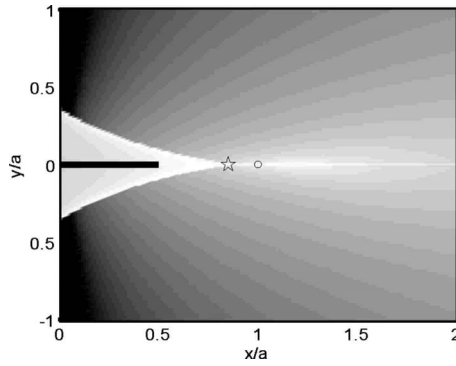


Fig. 4. Plot of the intensity outside the balloon predicted by ray tracing. The star indicates the location of the maximum intensity, and the circle marks the focal point predicted by the paraxial approximation. The bar spans the range of observed pressure maxima from 500 to 12 000 Hz using a 0.3 m balloon filled with carbon dioxide.

$$B_{00} = \frac{2\pi p_0 j_0(ka) + A_{00} h_n^{(1)'} - \Delta p}{j_0(k_b a)}, \quad (17)$$

$$B_{mn} = \frac{4\pi p_0 i^n j_n(ka) [Y_n^m(\phi_k, \theta_k)]^* + A_{mn} h_n^{(1)}(ka)}{j_n'(k_b a)}, \quad (18)$$

$(m, n \neq 0).$

The prime is used to denote differentiation with respect to the argument. These coefficients may be used to obtain plots of the total pressure field given by

$$p_e = p_i + p_s = \sum_{n=0}^{\infty} \sum_{m=-n}^n [4\pi p_0 i^n j_n(kr) [Y_n^m(\phi_k, \theta_k)]^* + A_{mn} h_n^{(1)}(kr)] Y_n^m(\phi, \theta) \quad (19)$$

for the region outside the balloon. The calculated sound pressure level results for the same regions as the experimental and numerical results are displayed in Figs. 2(e) and 2(f) for $ka=17.5$ and $ka=27.5$, respectively. The analytical and experimental results agree on the location of the focal region, which was not predicted by the lens equation or ray tracing. The results also agree on the number and locations of the lobes in the measurement window, beyond the slight shifting of the experimental data caused by balloon positioning error.

VI. DISCUSSION

The similarities between the results obtained from the experimental, numerical, and analytical results are apparent. Despite the reduction of the numerical experiment from three to two dimensions, the number and locations of the nodes of the field are strikingly similar to the experimental and analytical results. Further investigation of the analytical results reveals that only for $ka > 100$ does the balloon appear sufficiently large for the focal region to converge to that predicted by ray tracing.

The experimental results are compared with the predictions of the lens equation and the ray tracing method in Fig. 4. Because the lens equation and the ray tracing approach are independent of wavelength when they are valid, the axes of Fig. 4 are in terms of the radius of the sphere instead of the wavelength as is the case for the other plots. The plot shows

the intensity in arbitrary units as predicted by ray tracing. Although ray tracing, which removes the paraxial approximation, predicts that the focal region will move closer to the sphere and the spatial smearing of the focus, the predicted focus is too far from the sphere compared to the observed results. Also, the frequency dependent lobes apparent in Fig. 2 are absent because the ray tracing method is frequency independent.

Figure 3 illustrates the effect of the balloon on wave propagation for several values of ka . At the interface the reflected and transmitted portions of the incident wave are apparent. As the wave propagates past the balloon the shadow region becomes more apparent as the wavelength of the incident wave decreases. For long wavelengths the diffraction around the sphere is significant and the focal region is less defined. At higher frequencies the lobe patterns in the focal region are caused by interference of the transmitted portion of the wave. The shadow region is not well defined for low ka values, but becomes more visible as the frequency increases. Diffraction produces creeping waves which invade the shadow region, which is readily apparent only close to the balloon.

VII. CONCLUSION

The balloon lens represents an intriguing demonstration for science and physics students of all levels. Although the experimental results might be somewhat surprising when compared to the prediction based on a ball lens or ray tracing, the main features of the field are similar enough that the lens description provides a first-order approximation. Despite the fact that the “focal” region is not in the location predicted by the lens equation, an unaided ear can easily localize it, hence the demonstration’s appeal as an interactive museum display. For beginning physics students, a balloon “lens” provides an excellent hands-on experiment and an opportunity to think laterally between the behavior of waves in the familiar optical domain and the acoustical domain. The same phenomena, used as a laboratory problem, may provide undergraduate physics students with an opportunity to compare a straightforward numerical model to experimental observations and to observe the evolution of waves through media. It also provides more advanced students who are learning about acoustic, electromagnetic, or quantum scattering with a simple macroscopic demonstration of the phenomenon, which can aid in conceptualizing the mathematics.

ACKNOWLEDGMENTS

The authors would like to thank Cole Duke for his assistance in taking measurements, and the BYU Frontiers Mentorship for supporting this research.

^{a)}Currently at the University of Texas at Austin. Electronic mail: derekctomas@gmail.com

¹H. Kruglak and C. C. Kruse, “A visual method for demonstrating refraction of sound,” *Am. J. Phys.* **8**, 260–261 (1940).

²R. Reis, “Apparatus for teaching physics: A sound lens,” *Phys. Teach.* **6**(1), 40–41 (1968).

³B. A. Davy and D. T. Blackstock, “Measurements of the refraction and diffraction of a short N wave by a gas-filled soap bubble,” *J. Acoust. Soc. Am.* **49**(3B), 732–737 (1971).

⁴Exploratorium Network for Exhibit-based Teaching, (www.exploratorium.edu/cmp/exnet/exhibits/group9/conversation_piece/).

⁵Miguel C. Junger and David Feit, *Sound, Structures and Their Interaction*

2nd ed. (MIT, Cambridge, MA, 1986).

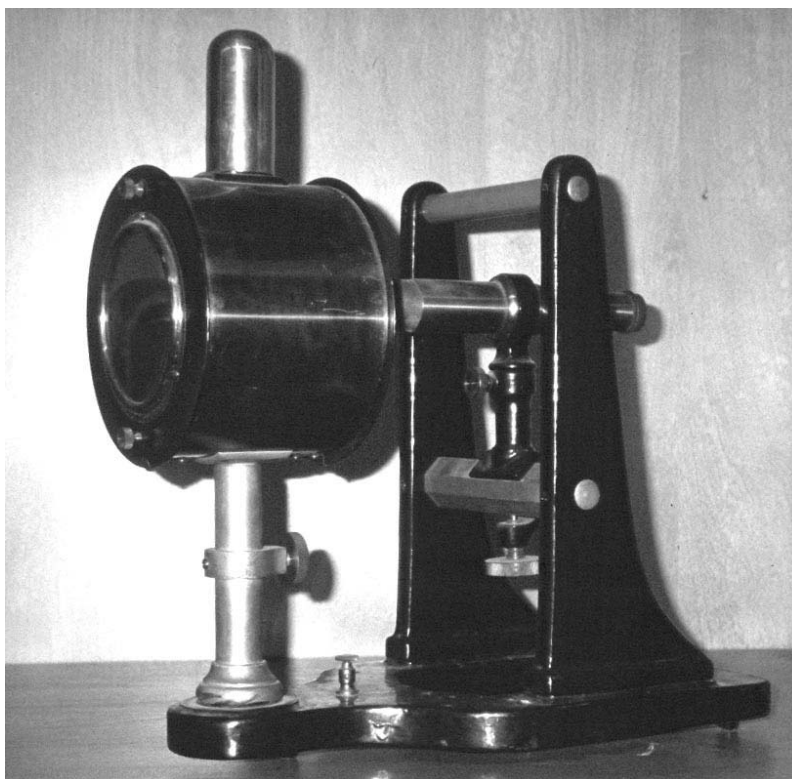
⁶Ross L. Spencer, "Manual for computational physics course at BYU," www.physics.byu.edu/Courses/Computational/phys430/phys430.pdf.

⁷Ranier Kress, "Acoustic scattering," in *Scattering and Inverse Scattering in Pure and Applied Science*, edited by E. R. Pike and Pierre C. Sabatier

(Academic, London, 2001).

⁸Allan D. Pierce, *Acoustics: An Introduction to Its Physical Principles and Applications* (Acoustical Society of America, Melville, NY, 1989).

⁹Mary L. Boas, *Mathematical Methods in the Physical Sciences* 3rd ed. (J Wiley, Hoboken, NJ, 2006).



Radio Electroscope. The new experimental science of radioactivity soon spawned its own technology. The favored detector was the electroscope and the electrometer; Cajorie, writing in *A History of Physics* (1929) about Marie Curie's work, noted that she was "working with the electrometer as the chemist works with the spectroscope" in her research. This Radio Electroscope appears in the flyer "Improved Physical Apparatus for Advanced Laboratory Work," published by the Gaertner Scientific Corporation of Chicago, ca. 1930, where it is listed at \$95.00. The electroscope leaves in the cylindrical metal case are observed with the microscope with the light scattered from the ground glass window. A shallow tray placed on a platform inside the cylinder holds the radioactive material. This apparatus is at Franklin and Marshall College in Lancaster, Pennsylvania in the Greenslade Collection. (Photograph and Notes by Thomas B. Greenslade, Jr., Kenyon College)